Comparative Biophysical Study of Meibomian Lipids of Wild Type and *Soat1*-Null Mice: Implications to Meibomian Gland Dysfunction and Dry Eye Disease

Xiaojie Xu,[1] Amber Wilkerson,[2] Guangle Li,[1] Igor A. Butovich,[2] and Yi Y. Zuo[1,3]

[1]Department of Mechanical Engineering, University of Hawaii at Manoa, Honolulu, Hawaii, United States
[2]Department of Ophthalmology and Graduate School of Biomedical Sciences, University of Texas Southwestern Medical Center, Dallas, Texas, United States
[3]Department of Pediatrics, John A. Burns School of Medicine, University of Hawaii, Honolulu, Hawaii, United States

Correspondence: Igor A. Butovich, 5323 Harry Hines Boulevard, Dallas, TX 75390, USA; igor.butovich@utsouthwestern.edu. Yi Y. Zuo, 2540 Dole St, Holmes Hall 302, Honolulu, HI 96822, USA; yzuo@hawaii.edu.

Received: May 4, 2023
Accepted: July 28, 2023
Published: August 16, 2023

Citation: Xu X, Wilkerson A, Li G, Butovich IA, Zuo YY. Comparative biophysical study of meibomian lipids of wild type and *Soat1*-null mice: Implications to meibomian gland dysfunction and dry eye disease. *Invest Ophthalmol Vis Sci.* 2023;64(11):20. https://doi.org/10.1167/iovs.64.11.20

Purpose. The biophysical roles of Meibomian lipids (MLs) played in health and meibomian gland dysfunction (MGD) are still unclear. The purpose of this research is to establish the composition-structure-functional correlations of the ML film (MLF) using *Soat1*-null mice and comprehensive in vitro biophysical simulations.

Methods. MLs were extracted from tarsal plates of wild type (WT) and *Soat1* knockout (KO) mice. The chemical composition of ML samples was characterized using liquid chromatography – mass spectrometry. Comprehensive biophysical studies of the MLFs, including their dynamic surface activity, interfacial rheology, evaporation resistance, and ultrastructure and topography, were performed with a novel experimental methodology called the constrained drop surfactometry.

Results. *Soat1* inactivation caused multiple alternations in the ML profile. Compared to their WT siblings, the MLs of KO mice were completely devoid of cholesteryl esters (CEs) longer than C_{18} to C_{20}, but contained 7 times more free cholesterol (Chl). Biophysical assays consistently suggested that the KO-MLF became stiffer than that of WT mice, revealed by reduced film compressibility, increased elastic modulus, and decreased loss tangent, thus causing more energy loss per blinking cycle of the MLF. Moreover, the KO mice showed thinning of their MLF, and reduced evaporation resistance.

Conclusions. These findings delineated the composition-structure-functional correlations of the MLF and suggested a potential biophysical function of long-chain CEs in optimizing the surface activity, interfacial rheology, and evaporation resistance of the MLF. This study may provide novel implications to pathophysiological and translational understanding of MGD and dry eye disease.

Keywords: meibomian lipid (ML), dry eye disease (DED), cholesteryl ester (CE), surface tension, constrained drop surfactometry

Holocrine meibomian glands (MGs) are specialized glands that are embedded in the upper and lower tarsal plates of the eyelids of humans and most mammals.[1] The main function of MGs is to produce a lipid-rich secretion, also known as meibum, which is expressed through the set of ducts and orifices onto the ocular surface, where, after being mixed with aqueous tears, participates in the formation of a dynamic, ever-changing, multilayered structure called the tear film (TF).[1] The exact structure of the TF is a subject of undergoing studies.[2–5] However, a predominant view is that meibum forms its outermost sublayer called the TF lipid layer (TFLL), whose main function is believed to be reducing evaporation of the TF.[6–9] Alterations in the TFLL may lead to TF instability and a loss of its protective function – an often-observed condition associated with various types of MG dysfunction (MGD) and dry eye disease (DED).[10,11] The major causes of these pathological conditions are a change in expressibility of meibum from the orifices due to its inspissation, changes in the ability of meibum to form TFLL, physical obstruction of MG ducts/orifices due to, for example, hyperkeratinization, or insufficient production of meibum in MGs due to MG dropout. The first two causes are closely related to alterations in the chemical composition of meibum, which is formed, predominantly, from wax esters (WEs, about 41% of all lipids), cholesteryl esters (CEs, 31%), (O-acyl)-ω-hydroxy fatty acids (OAHFAs), and a number of other classes of lipids.[6,12–14] The balance between these groups of lipids is absolutely essential for maintaining the health of the ocular surface and adnexa, as a number of studies with genetically modified gene knockout (KO) mice demonstrated severe ocular abnormalities once biosynthesis of any of those lipids had been arrested.[15–17] Specifically, inactivation of the *Soat1* gene led to a complete stoppage of CE production in MGs and a severe change in the eye phenotype in experimental animals.[18–20] In addition, noted were changes in meibum thermotropic characteristics,

such as a multi-degree increase in its melting temperature, which affected its expressibility from MGs.[21] However, no other characterization of the biophysical/physicochemical properties of meibomian lipids (MLs) of *Soat1*$^{+/-}$ mice was conducted.

In this paper, we report results of a comprehensive biophysical study of the dynamic surface activity, interfacial rheology, evaporation resistance, and ultrastructure of the ML films (MLFs) extracted from wild type (WT) and *Soat1* KO mice, using a novel experimental methodology called the constrained drop surfactometry (CDS). The CDS is a new generation of droplet-based tensiometry technique initially developed in our laboratory for studying the biophysical properties of pulmonary surfactants.[22] Given the biophysical similarities between pulmonary surfactant and the TFLL,[23] we have recently modified the CDS to make it an ideal and versatile in vitro model for studying the biophysics of the TFLL.[24–27] By correlating the lipidomic analysis and biophysical assays of the MLs of WT and *Soat1* KO mice, our study revealed novel experimental evidence on the composition-structure-functional correlations between nonpolar lipid components in the MLF and its biophysical properties. These results may provide novel insights into the pathophysiology of MGD and DED, and biophysical behavior of the TF and TFLL.

Methods

Reagents

Lipid standards were purchased from Avanti Polar Lipids (Birmingham, AL, USA), MilliporeSigma (St. Louis, MO, USA), and NuChek Prep. (Elysian, MN, USA). Acetonitrile, *iso*-propanol, chloroform, and methanol of chromatography- or mass-spectrometry-grade were purchased from MilliporeSigma and Thermo Fisher Scientific (Waltham, MA, USA). Compressed gasses (helium and nitrogen of ultra-high purity) were obtained from Airgas (Dallas, TX, USA). Acetic and formic acids (each >99.9% purity), anhydrous ammonium formate (>99.995%), and leucine-enkephalin were purchased from MilliporeSigma.

Mouse Meibomian Lipids

All animal procedures used in this study were approved by the Institutional Animal Care and Use Committee of the University of Texas Southwestern Medical Center and were conducted in accordance with the Association for Research in Vision and Ophthalmology Statement for the Use of Animals in Ophthalmic and Vision Research. *Soat1*$^{+/-}$ founder mice on a C57BL/6J background were purchased from the Jackson Laboratory (B6.129S4-*Soat1*^{tm1Far}/Pgn, Stock #007147; Bar Harbor, ME, USA). The targeted mutation resulted in *Soat1*-null mice, which do not have SOAT1 protein detected by immunoblotting samples from preputial gland, ovaries, and adrenals of these mice. MLs were extracted from the tarsal plates of WT and KO mice by following procedures detailed elsewhere.[19] Four tarsal plates from each mouse were excised from the eyelids, dissected free from epidermis, and placed in glass vials filled with approximately 0.5 mL of chloroform:methanol (*v/v* 2:1) for overnight extraction in a refrigerator. The lipids were repetitively extracted with 3 × 1 mL of the solvent mixture, and the extracts were pooled. To collect enough lipid material for biophysical evaluation, ML samples from three male WT mice and three male KO mice were combined in glass vials to produce two pooled WT and KO ML study samples. Then, the samples were dried under a stream of nitrogen and weighed on an analytical microbalance, to produce pooled off-whitish-to-yellowish oily samples of sufficient physical size of about 0.5 mg each, and compared using ultrahigh-pressure liquid chromatography-mass spectrometry (UHPLC-MS; see lipidomic analysis below). The solvent was evaporated under a gentle stream of nitrogen. The remaining lipid materials were sealed and stored at −20°C until analyses.

Lipidomic Analysis

ML samples were analyzed using UHPLC-MS. The liquid chromatography (LC) instrument was a Waters M-Class UHPLC binary system (Waters Corp., Milford, MA, USA). Separation of lipids was conducted on an Acquity C8-BEH UHPLC column (2.0 mm × 100 mm, 1.7 µm) using isocratic elution with a 95% isopropanol: 5% acetonitrile (each with 5% of 10 mM aqueous ammonium formate as additive) solvent mixture as described before.[19] The elutions were conducted at a flow rate of 20 µL/min, with a column temperature of 35°C. The MS instrument was a high resolution quadrupole Time-of-Flight Synapt G2-Si system equipped with a ZSpray atmospheric pressure ionization LC interface, an IonSabre-II atmospheric pressure chemical ionization (APCI) ion source and a LockSpray unit. The LockSpray was used with a 2 µg/mL Leucine-Enkephalin solution in 50% H_2O: 50% acetonitrile: 0.1% formic acid as calibrant (Waters Corp.). The lipid analytes were detected in positive ion mode as prominent $(M + H)^+$, $(M - H_2O + H)^+$, and $(M -$ fatty acid $+ H)^+$ adducts. The APCI detector was used with the following settings: mode "Sensitivity"; resolution 10,000 FWHP; scan rate 1 scan/sec; corona current 1.7 µA; probe temperature 350°C; source temperature 150°C; sampling cone 30 V; cone gas flow (nitrogen) 100 L/hour; desolvation gas flow 400 L/hour; nebulizer gas pressure 3 bar; and the trap gas flow (ultra-high purity helium) 2 mL/min. The accuracy of measured *m/z* values for lipid analytes was better than 5 mDa.

The UHPLC-MS raw data were analyzed with the MassLynx version 4.1 software package (Waters Corp.). The total ion chromatograms (TICs) and extracted ion chromatograms (EICs) were used to estimate, respectively, the total lipid content and the apparent abundances of individual analytes, as described before.[19] Briefly, the signals for EIC were extracted with a mass window of 10 mDa, plotted, and integrated using the MassLynx's Integration routine. The results were statistically analyzed with the SigmaStat version 3.5 software (Systat Software, San Jose, CA, USA). Reproducibility of the analyses was established in a series of repetitive injections of samples and standard lipids as described earlier[28] and found to be better than ±5%.

Dynamic Surface Activity

Dynamic surface activity of the mouse MLF was studied with CDS,[22,24] in which the MLF film can be spread at the air-water surface of an approximately 4 mm sessile drop enclosed in an environmental control chamber. As shown in Figure 1, the MLF is constrained at the air-water surface of the sessile drop using a pedestal with knife-sharp edges. The MLF film can be compressed and expanded by regulating the surface area of the droplet using closed-loop axisymmetric

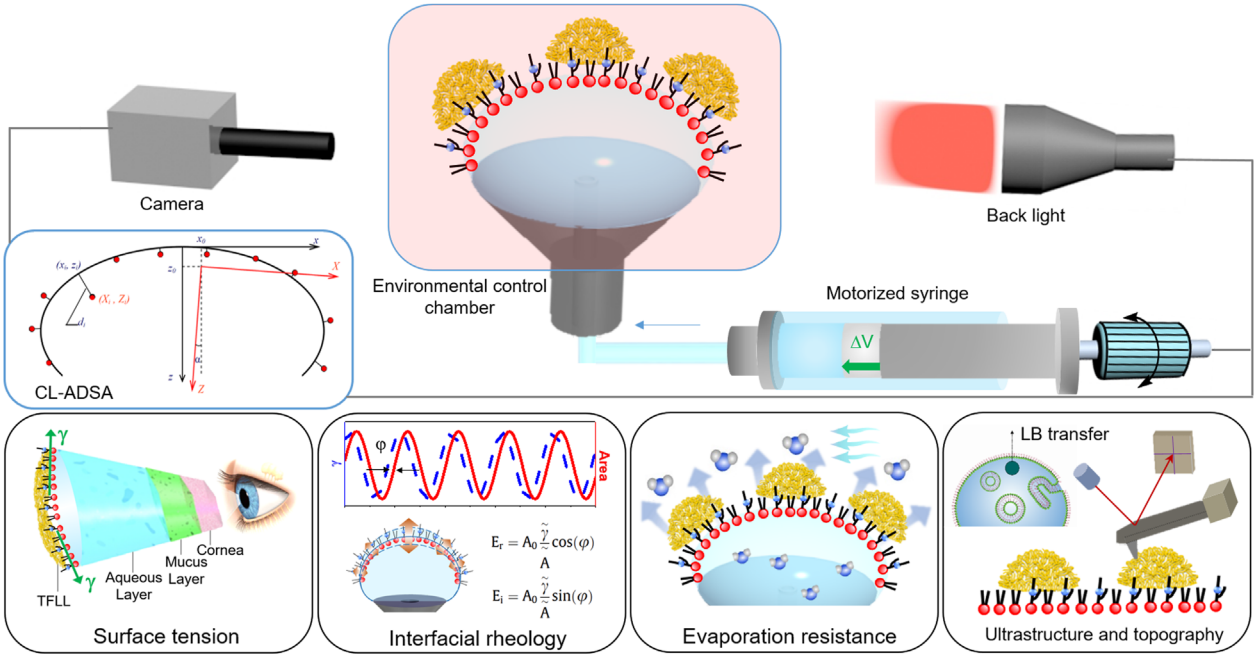

Figure 1. Schematics of the constrained drop surfactometry (CDS) as a versatile biophysical model for studying mouse MLFs. The CDS uses the air-water surface of a 4-mm sessile drop, constrained on a carefully machined pedestal with knife-sharp edges, to accommodate the spread MLF. The droplet is enclosed in an environmental control chamber that maintains a constant temperature, relative humidity, and ambient airflow rate. The spread MLF can be compressed and expanded at a highly dynamic rate of 20% relative area per second to simulate a blink, by regulating fluid flow into and out of the droplet using a motorized syringe. Dynamic surface tension of the film is determined with closed-loop axisymmetric drop shape analysis (CL-ADSA), which measures surface tension of the film remotely by analyzing the shape of the MLF-covered droplet in real-time. The CDS is capable of multiple biophysical assays of the MLFs, including dynamic surface tension, interfacial dilational rheology, evaporation resistance, and ultrastructure and topography of the MLFs when being used in conjunction with the Langmuir-Blodgett (LB) technique and atomic force microscopy (AFM).

drop shape analysis (CL-ADSA),[29] which determines surface tension from the shape of the droplet. Surface pressure presents the differences between the surface tension of the clean air-water surface and that of the MLF-covered surface.

Specifically, approximately 0.1 µL mouse ML samples at approximately 1 mg/mL lipid concentration were spread onto the droplet surface, and left for 1 minute to allow solvent evaporation. The spread MLF was compressed to 30% of its initial surface area, at a rate of 20% relative area per second (A%/s), corresponding to 0.1 cm^2/s, at 34.0 ± 0.1°C. At least five compression-expansion cycles were studied, and the fifth cycle was analyzed as representative. Dynamic surface activity of the MLF was quantified with the average film compressibility $\kappa = \frac{1}{A}\frac{\partial A}{\partial \gamma}$, and the hysteresis area of the compression-expansion loop.

Surface Dilational Rheology

Protocols for determining the surface dilational modulus $E = \frac{d\gamma}{dlnA}$ of the mouse MLF can be found elsewhere.[24,30] Briefly, the surface area of the MLF film was made to undergo a small-amplitude (i.e. amplitude < 10%) harmonic oscillation (i.e. sinusoidal waveform) with frequencies from 0.01 to 0.25 Hz, at 34.0 ± 0.1°C. The elastic modulus (E_r) and the viscous modulus (E_i) were determined from the phase shift (φ) between the surface area and the surface tension waveforms. The ratio between E_i and E_r defines the loss tangent (tanφ).

Evaporation Resistance

Evaporation resistance of the mouse MLF was evaluated with a ventilated and closed-chamber evaporimeter recently developed in our laboratory.[26] As shown in Figure 1, this novel in vitro evaporimeter was designed based on the CDS. While studying water evaporation, the surface area of the droplet (A_{drop}) was maintained constant at 0.35 ± 0.01 cm^2 by automatically compensating the evaporated water with injection ($\Delta V/\Delta t$) into the droplet within a time period of 5 minutes. The evaporation rate (mm/min) was calculated with $(\Delta V/\Delta t)/A_{drop}$. The relative humidity, temperature, and airflow rate were controlled at 33.0 ± 2.0%, 34.0 ± 0.1°C, and 1.0 ± 0.1 m/s, respectively. The volumetric evaporation rate for a pure water droplet, without any lipid or surfactant film at the air-water surface, was found to be less than 2.7 µL/min, in the similar range of the basal tear production of healthy adults.[31,32]

Ultrastructure and Film Topography

Ultrastructure and topography of the mouse MLF were studied with combined Langmuir-Blodgett (LB) transfer technique and atomic force microscopy (AFM).[25] Plenty of experimental evidence has demonstrated that when being operated properly, the LB film transferred to a solid substrate is able to reserve the lateral structure and topography of the film at the air-water surface.[33,34] The MLF was first LB transferred to a freshly peeled mica sheet, and was then scanned

Investigative Ophthalmology & Visual Science

in air with the tapping mode using an Innova AFM (Bruker, Santa Barbara, CA, USA).

Statistical Analysis

Results were shown as mean ± SD ($n \geq 3$). One-way ANOVA with Tukey's means comparison test was used to determine differences between groups (OriginPro, Northampton, MA, USA). A $P < 0.05$ was considered to be statistically significant.

Results

Lipidomic Characterization of the Mouse Meibomian Samples

Figure 2 shows the lipidomic characterization of the ML samples extracted from the WT and KO mice. Compared with WT mice, the mutation resulted in a moderate 27% reduction in the total amount of produced MLs. Moreover, *Soat1* inactivation caused multiple changes in the composition of the meibomian lipidome of the KO mice, such as a 51% increase in the apparent abundance of triacylglycerols (TAGs), and a 39% decrease in total WEs (see Fig. 2a). Most importantly, the pool of Chl rose 7 times in the KO mice compared with their WT siblings, and, corroborating our previous results,[19] an almost complete removal of CEs longer than C_{18} to C_{20} was observed (see Fig. 2b). These changes transformed Chl into the main, most abundant lipid species produced by *Soat1*-null MGs with the apparent abundance of approximately 50% in the tested pool of lipids. Simultaneously, the apparent abundance of CEs dropped from 38% to 1.5% or so, of which all CEs were of shorter chains in nature. Other changes were an apparent decline in the WE content from 38% to 23%, and an increase in the TAG fraction from 17% to 23%.

Dynamic Surface Activity of the Mouse Meibomian Lipid Films

Figure 3 shows the comparison of dynamic surface activity of the MLF between WT and KO mice at the physiologically relevant temperature of 34°C. Figure 3a shows the typical compression-expansion isotherms of these two MLFs. Reproducibility of the compression-expansion isotherms can be found in Supplementary Figure S1 of the Supporting Information. It can be seen that both WT and KO MLFs can be compressed to a maximum surface pressure of approximately 50 mN/m, corresponding to a minimum surface tension of approximately 20 mN/m. However, as shown in Figure 3b, the compressibility (κ) of the KO MLF is lower than that of the WT MLF (1.33 vs. 1.75 m/mN), indicating that the MLF of KO mice is less compressible, or in other words, "harder" than the MLF of WT mice. Most importantly, as shown in Figure 3c, the hysteresis area of the KO MLF is found to be significantly larger than that of the WT MLF (0.13 vs. 0.37 μJ per cycle). The hysteresis area of a compression-expansion cycle indicates energy loss per cycle.[35] Hence, our results suggest that the energy loss per compression-expansion cycle for the MLF of KO mice is three times that of the healthy WT mice.

Interfacial Rheology of the Mouse Meibomian Lipid Films

Figure 4 shows the dilational rheological properties of the MLFs of the WT and KO mice. All rheological properties were determined at 34°C and a characteristic surface pressure of 30 mN/m, corresponding to the surface tension of whole tear.[24,36] As shown in Figure 4a, the elastic modulus (E_r) of the KO MLF almost doubles that of the WT MLF at all tested frequencies, from 0.01 to 0.25 Hz, thus indicating that the MLF of the KO mice is significantly stiffer or more rigid than the WT mice. This conclusion is also consistent with the compressibility measurement shown in Figure 3b. Figure 4b shows the viscous modulus (E_i) of the MLFs. In comparison to the E_r measurements shown in Figure 4a, the E_i of all MLFs is significantly smaller than the corresponding E_r, indicating that these MLFs are essentially more elastic than viscous. Moreover, the E_i of the KO MLF is higher than that of the WT MLF at all tested frequencies. Most importantly, as shown in Figure 4c, it is found that the loss tangent ($\tan\varphi = E_i/E_r$) of the KO MLF is in general smaller than that of the WT MLF. In addition, the $\tan\varphi$ of both WT and KO

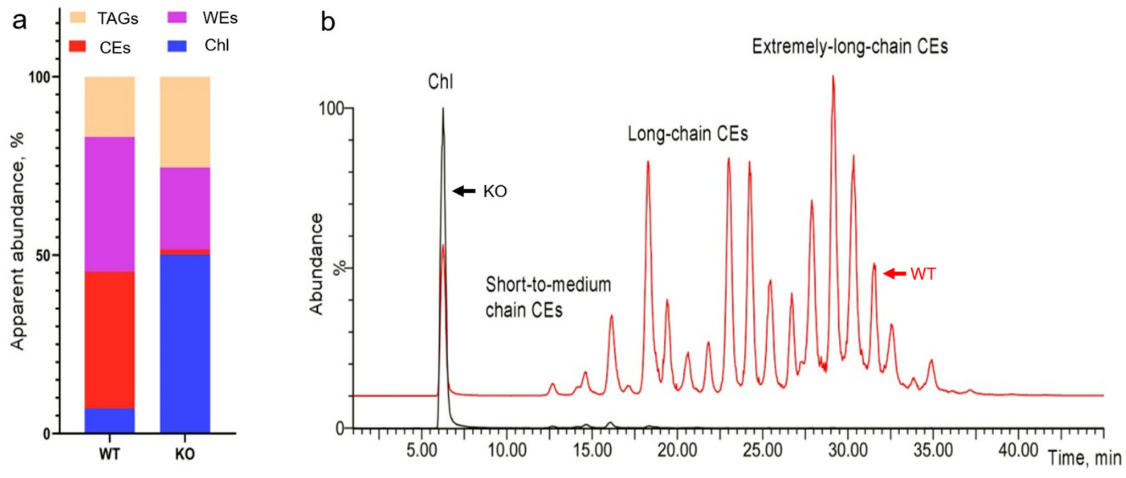

Figure 2. Ultrahigh-pressure liquid chromatography–mass spectrometry (UHPLC-MS) lipidomic characterization of the meibomian samples extracted from wild-type (WT) and *Soat1*-knockout (KO) mice. (a) Compositions of the MLs extracted from WT and KO mice. (b) Effect of *Soat1* inactivation on the ML profiles of mice. Note the major shifts in the Chl/CE ratio in the KO MLs, and a much subtler effect of the mutation on TAGs and WEs.

Investigative Ophthalmology & Visual Science

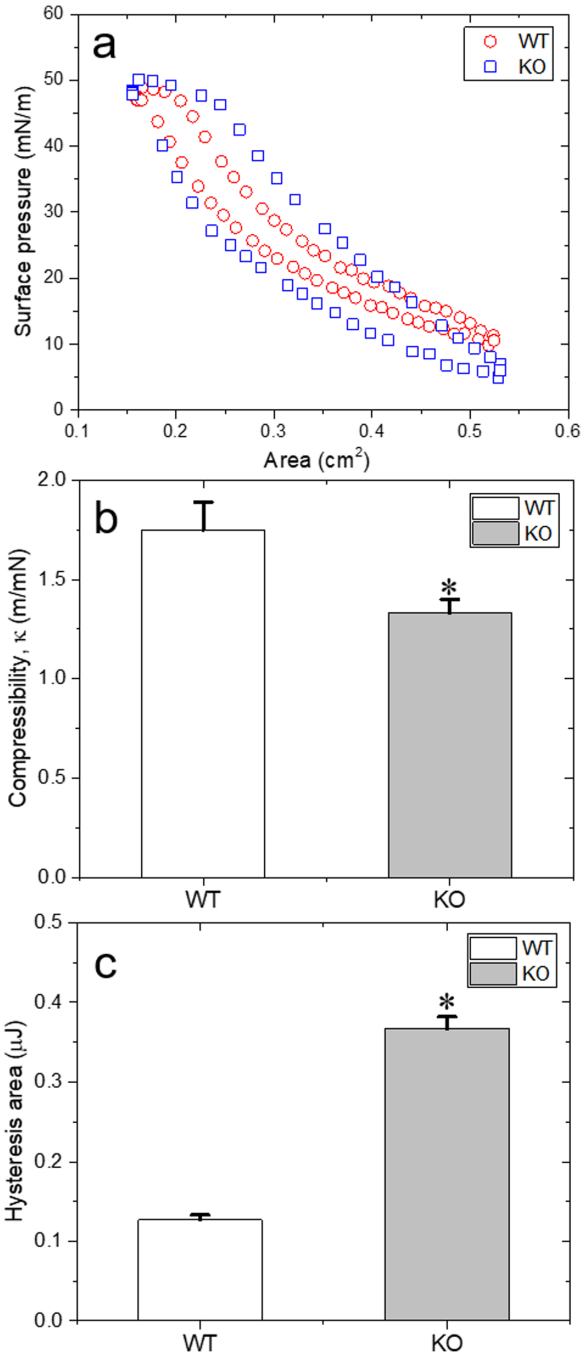

Figure 3. Dynamic surface activity of the MLFs of WT and KO mice at 34°C. (**a**) Typical compression-expansion isotherms of the WT and KO MLFs. (**b**) Statistical analysis of the compressibility (κ) of the WT and KO MLFs. (**c**) Statistical analysis of the hysteresis area, that is, the energy loss per cycle, for the WT and KO MLFs. *$P < 0.05$ represents statistically significant differences.

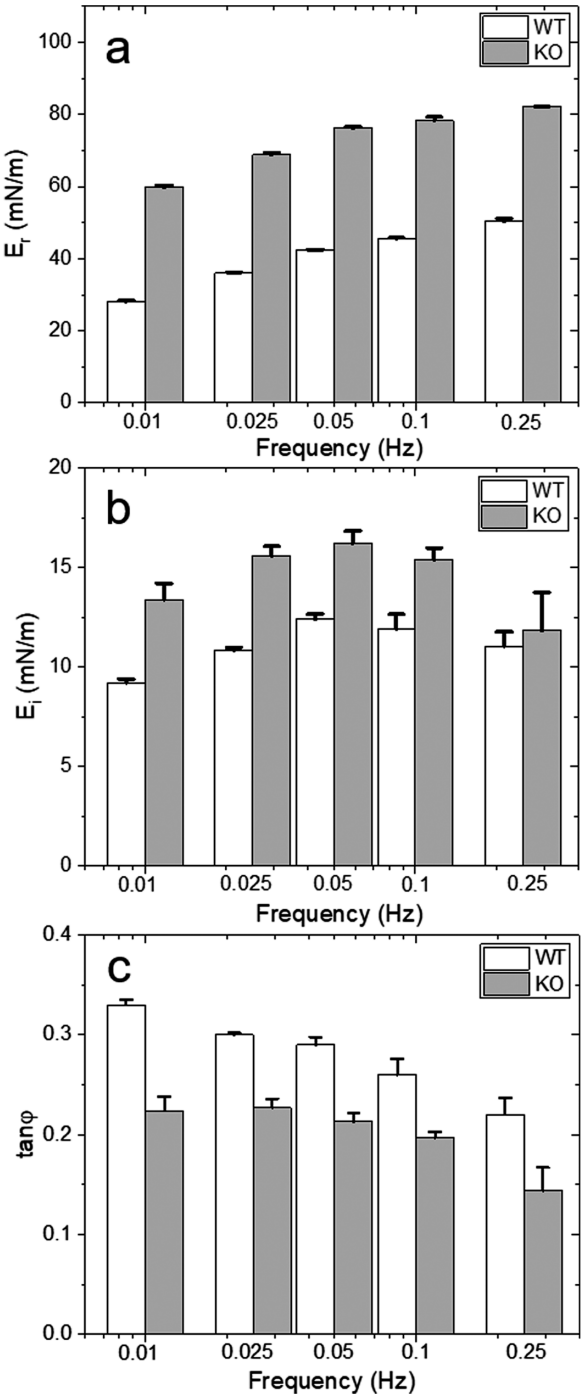

Figure 4. Interfacial dilational rheological properties of the MLFs of WT and KO mice. (**a**) Elastic modulus (E_r) of the WT and KO MLFs. (**b**) Viscous modulus (E_i) of the WT and KO MLFs. (**c**) Loss tangent (tanφ) of the WT and KO MLFs. All interfacial rheological properties were determined at the characteristic surface pressure of 30 mN/m at 34°C.

MLFs appears to decrease with increasing frequency, which is consistent with the frequency-dependence of the phospholipid film but has an opposite frequency-dependence as a simplified model TF lipid layer consisting of behenyl oleate (BO), cholesteryl oleate (CO), phosphatidylcholine (PC), and palmitic-acid-9-hydroxy-stearic-acid (PAHSA; 40:40:15:5, respectively).[24]

Evaporation Resistance of the Mouse Meibomian Lipid Films

Figure 5 shows the evaporation resistance of the MLFs of the WT and KO mice, upon increasing surface pressure of these MLFs. It can be seen that both WT and KO MLFs demonstrate statistically significant resistance to water evaporation, and

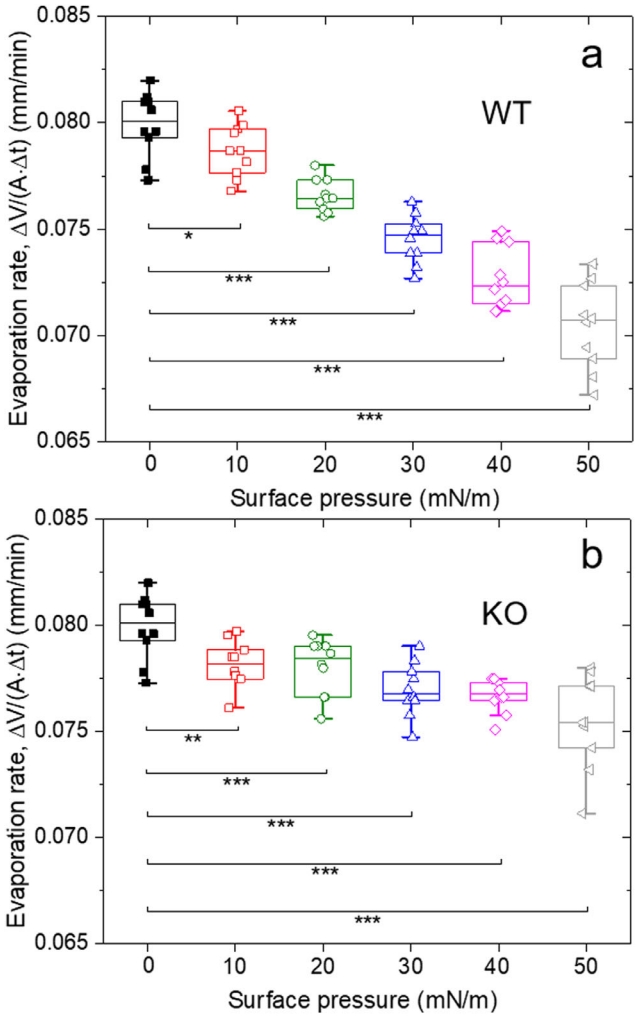

Figure 5. Effects of the MLFs of WT (**a**) and KO (**b**) mice, under various surface pressures, on water evaporation. $^{*}P < 0.05$, $^{**}P < 0.01$, and $^{***}P < 0.001$.

the evaporation resistance increases with increasing surface pressure of the MLFs. Nevertheless, the MLF of the WT mice shows significantly higher resistance to water evaporation than the MLF of the KO mice, especially at high surface pressures. For instance, at 30 mN/m, the MLFs of the WT and KO mice reduce the water evaporation rate by 6.8% and 3.7%, respectively. At 50 mN/m, however, the MLFs of the WT and KO mice reduce the water evaporation rate by 11.9% and 5.6%, respectively, thus indicating that the evaporation resistance of the WT MLF more than doubles that of the KO MLF at this high surface pressure. In fact, linear regression of the data shown in Figure 5 indicates that the dependence of the evaporation resistance on surface pressure for the WT MLF more than doubles that of the KO MLF, indicating that the MLF of WT mice has a much better retardation effect to water evaporation than the MLF of KO mice.

Ultrastructure and Topography of the Mouse Meibomian Lipid Films

Figure 6 shows the ultrastructure and topography of the MLFs of WT and KO mice, at 3 characteristic surface pressures, that is, 20, 30, and 40 mN/m, obtained at 34°C. Reproducibility of these AFM images can be found in Supplementary Figures S2–S7. As shown in Figure 6a, the WT MLF at a low surface pressure of 20 mN/m demonstrates a multilayered structure with a network of lipid folds 40 to 60 nm in height. This structure is very different from that of the simplified model TFLL investigated in our previous studies.[25,26] Single-component or four-component model lipid films at such low surface pressures typically exhibit a monolayer conformation.[25,26] With increasing surface pressure to 30 mN/m (see Fig. 6b), the WT MLF shows discrete bead-like structures, with a lateral diameter of approximately 1.4 µm and a height of approximately 15 nm, surrounded by coffee-ring-like structures of approximately 3 µm in diameter and approximately 4 nm in height. A similar structure has been detected in the model TFLL of BO:CO:PC:PAHSA (40:40:15:5, respectively) at the same surface pressure.[26] These bead-like structures are most likely formed by squeezed out nonpolar lipids in the MLF, due to their lack of affinity to the air-water surface. The height of the coffee-ring-like structures closely matches the thickness of fully hydrated lipid bilayers (i.e. approximately 4 nm).[37] Hence, they are most likely formed by dewetting-driven self-assembly of reverse micelles of polar lipids mixed with nonpolar lipids.[26] With further increasing the surface pressure to 40 mN/m (see Fig. 6c), the WT MLF is compressed into a lipid multilayer consisting of a compacted bilayer (approximately 4 nm in height) and large aggregates of 50 to 100 nm in height atop the compacted bilayer.

The MLF of the KO mice shows a completely different ultrastructure and topography in comparison to that of the WT mice. As shown in Figure 6d, the KO MLF at the low surface pressure of 20 mN/m shows only limited amounts of multilayered protrusions 10 to 30 nm in height. At 30 mN/m (see Fig. 6e), a large portion of the film is still covered with a monolayer, whereas only isolated multilayer protrusions appear in the MLF. At 40 mN/m (see Fig. 6f), the KO MLF still appears to be mostly in a monolayer conformation without significant amounts of multilayered structures detected even at this high surface pressure. Neither bead-like structures nor coffee-ring-like structures, as appearing in the WT MLF, are detected in the KO MLF. These structural variations are consistent with the compositional variations of the MLFs of the WT and KO mice, because the KO MLF lacks the most important nonpolar lipid, that is, CEs, but is enriched in Chl.

Discussion

Composition-Structure-Functional Correlations Revealed by Comparison of the Meibomian Lipid Films Between WT and *Soat1*-Null Mice

Corroborating our previous result,[19] inactivation of *Soat1* almost completely eliminated long- and extremely long-chain CEs from meibum, and led to a multifold increase in non-esterified free Chl (see Fig. 2). The remaining CEs were based on C_{14} to C_{18} fatty acids with 1, 2, or 3 double bonds, that is, similar to those found in serum of mice and humans. As a result of this, free Chl became the major lipid species found in ML of the *Soat1*-null mice, comprising $\geq$ 50% of the lipid pool. It is well known that Chl has a profound impact on the ML phase behavior.[38] Hence, it is not unexpected that enrichment of lipid mixtures (such as MLs) with Chl would noticeably change their rheological/thixotropic properties, especially at the physiologically relevant temperature around 34°C.

Investigative Ophthalmology & Visual Science

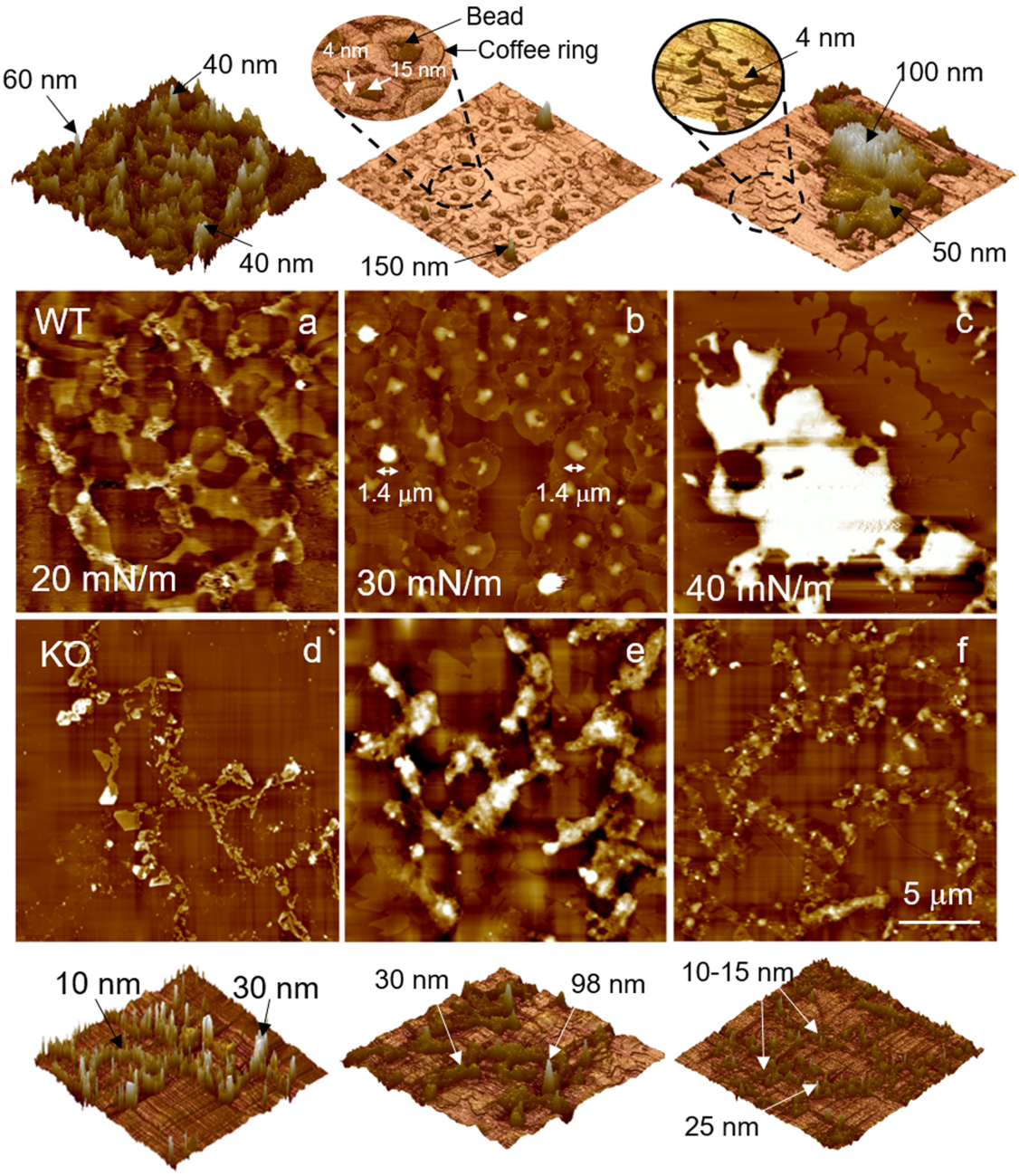

Figure 6. Ultrastructure and topography of the MLFs of WT (**a-c**) and KO (**d-f**) mice at three characteristic surface pressures, that is, 20, 30, and 40 mN/m. All AFM images shown in the 2 middle rows have the same scanning area of 20 × 20 μm, and the same *z* range of 50 nm. Images in the top and bottom rows show the 3D renderings of the WT and KO MLFs, respectively. *Single-headed arrows* indicate the heights of the structures, while *double-headed arrows* indicate the lateral dimensions of the structures. The bar represents 5 μm.

Indeed, in comparison to the MLF of healthy WT mice, we found multiple biophysical variations to the MLF of KO mice, and such biophysical variations appear to be closely correlated with the alternation of the ML profile. Both surface tension and interfacial rheological measurements consistently suggested that the MLF of KO mice is stiffer than the MLF of WT mice, revealed by the reduced film compressibility (see Fig. 3b), increased elastic modulus (see Fig. 4a), and decreased loss tangent (see Fig. 4c) of the KO MLF. These biophysical variations can be correlated with the dramatic increase of free Chl in the ML samples of KO mice. How does Chl affect the phase behavior of lipid monolayers and bilayers largely depends on the temperature and the molar fraction of Chl in the mixture.[39] The overall biophysical effect of Chl is to fluidize lipids in a rigid gel phase by disrupting lipid packing, or to condense lipids in a fluid phase by interacting with their disordered chains and thus stabilizing the fluid lipids.[40–43] At 34°C, most lipids in meibum, especially those with relatively shorter fatty acid chains (C_{14}-C_{18}), exist in a fluid phase. Hence, the increased Chl fraction in ML of KO mice is expected to condense and rigidify the MLF. One direct adverse biophysical consequence of increasing film rigidity is to cause more energy loss per compression-expansion cycle that mimics the blinking cycle

of the MLF (see Fig. 3c). Indicatively, thermotropic transitions in meibum of *Soat1*-null mice were distinctively different from those of WT mice.[19] The melting transition of KO meibum, which began at −10°C similarly to WT meibum, started to deviate from the trajectory of WT meibum after reaching a normal physiological temperature of cornea of around 34°C, at which only a portion of the KO meibum melted, whereas the other part remains solidified, which is consistent with a large presence of high-melting fraction of free Chl. In terms of interfacial rheological properties, such a phase-mixing KO MLF demonstrates a decreased loss tangent in comparison to the WT MLF (see Fig. 4c).

The MLF formed from the CE-depleted/Chl-enriched KO mouse meibum seems to replicate many features of MLFs formed of human meibum with increased levels of Chl.[38] The in vitro surface activity and interfacial rheological properties of human meibum have been extensively studied by Fuller and coworkers.[44–46] Direct comparison of their results to the present study, however, is complicated by the different technical details used in these studies. Primarily relying on the Langmuir film balance, previous studies mostly focused on the MLFs at low surface pressures (less than 20 mN/m).[44,45] In contrast, the use of CDS allows us to scrutinize the MLFs under high surface pressures (20–40 mN/m), which are likely more relevant to the tear film in vivo.[23,35] In addition, whereas previous studies measured the interfacial shear rheology of the MLFs, we have studied the interfacial dilational rheology of the MLFs. The shear rheology studies changes in shape at a constant surface area, which provides information on the stability of the MLFs. In contrast, the dilational rheology determines changes in an area at a constant shape, which provides information about the composition of the MLFs.[30,47] Nevertheless, it was found that in comparison to ML samples extracted from healthy individuals, the MLFs of patients with MGD demonstrated a shorter film stability, modified rheological properties, and heterogeneous and patchy morphology at the air-water surface.[48]

Directly imaging the MLFs of WT and KO mice using AFM revealed further evidence about the composition-structure-functional correlations. The MLF of WT mice mostly depicts a multilayer conformation (see Figs. 6a-c). Especially at the physiologically relevant high surface pressures, for example, 40 mN/m, the MLF consists of a compacted bilayer (approximately 4 nm in height) and large aggregates of 50 to 100 nm in height atop the compacted bilayer (see Fig. 6c). In contrast, the multilayer structures largely, if not completely, disappear from the MLF of KO mice (see Figs. 6d-f). Thinning of the MLF for the KO mice is most likely related to the depletion of CEs from meibum, because our previous studies suggested that the multilayer structures are mostly composed of nonpolar lipids,[26] which can be easily squeezed out of the interfacial film at high surface pressure, because of their low affinity to the air-water surface. Interestingly, the same type of thinning of the MLF was also observed for human samples enriched with Chl,[38] thus indicating that the enrichment of Chl in the KO mouse sample may also contribute to the transition from multilayer to monolayers.

Implications to Meibomian Gland Dysfunction and Dry Eye Disease

Meibomian gland dysfunction (MGD) is the leading cause of DED.[49,50] It is believed that alteration of the ML profile, especially those nonpolar lipids in MLs, may significantly compromise the evaporation resistance of TFLL, thus leading to DED.[15,16] Although the alteration in the ML profile at MGD might be different from that observed here between the WT and KO mice, the present study shows that at the physiologically relevant high surface pressures, the evaporation resistance of the WT MLF more than doubles that of the KO MLF (see Fig. 5). In addition, the dependence of the evaporation resistance on surface pressure for the WT MLF also more than doubles that of the KO MLF, indicating that the MLF of WT mice has a much better retardation effect on water evaporation than the MLF of the KO mice (see Fig. 5). These data suggest that long- and extremely long-chain CEs, that is, those longer than C_{18} to C_{20}, may play an important role in reducing tear evaporation. Another factor to consider is the effect of accumulation of Chl in meibum. Being an amphiphilic compound with a high melting temperature, Chl mixed well with Meibomian lipids causes an increase in their melting temperature, and rigidity and collapsibility of Chl-enriched MLF.[19,38] Clinical studies linked hypercholesterolemia and MGD.[51–53] Considering that blood Chl can be transported to, and accumulated in, MGs in unaltered form, these observations provide an opportunity for Chl to play a role in inspissation of meibum of certain types of MGD (e.g. its obstructive variant) and patients with DED, and poor stability of their TF.[54,55] We are confident that future experiments with MLF will reveal the intricate mechanisms of molecular interactions between different types of Meibomian lipids, and their impact on the ocular surface homeostasis in the norm and pathology.

Conclusions

Using a novel experimental methodology called the constrained drop surfactometry (CDS), we reported a comprehensive biophysical study of the dynamic surface activity, interfacial rheology, evaporation resistance, and ultrastructure of the MLFs extracted from WT and *Soat*1 KO mice. By correlating the lipidomic analysis and biophysical assays of the MLs of WT and KO mice, our study revealed novel experimental evidence on the composition-structure-functional correlations of the MLFs, and suggested a potential biophysical function of long-chain CEs in optimizing the surface activity, interfacial rheology, and evaporation resistance of the MLFs. This study may provide novel implications to pathophysiological and translational understanding of MGD and DED.

Acknowledgments

Supported by National Institutes of Health (NIH) grant number R01 EY027349 (to I.A.B.), NSF grant number CBET-2011317 (to Y.Y.Z.), and Mary & Paul Wagner Blindness Prevention Fund of the Hawai'i Community Foundation grant number 20ADVC-102168 (to Y.Y.Z.).

Disclosure: **X. Xu**, None; **A. Wilkerson**, None; **G. Li**, None; **I.A. Butovich**, None; **Y.Y. Zuo**, None

References

1. Butovich IA. Meibomian glands, meibum, and meibogenesis. *Exp Eye Res*. 2017;163:2–16.
2. King-Smith PE, Fink BA, Hill RM, Koelling KW, Tiffany JM. The thickness of the tear film. *Curr Eye Res*. 2004;29:357–368.

Investigative Ophthalmology & Visual Science

3. Butovich I. Biochemistry and biophysics of human and animal tear film lipid layer: from composition to structure to function. *Invest Ophthalmol Vis Sci*. 2010;51:4154–4154.
4. Georgiev GA, Eftimov P, Yokoi N. Structure-function relationship of tear film lipid layer: a contemporary perspective. *Exp Eye Res*. 2017;163:17–28.
5. Cwiklik L. Tear film lipid layer: a molecular level view. *Biochim Biophys Acta*. 2016;1858:2421–2430.
6. Butovich IA. Tear film lipids. *Exp Eye Res*. 2013;117:4–27.
7. King-Smith PE, Bailey MD, Braun RJ. Four characteristics and a model of an effective tear film lipid layer (TFLL). *Ocul Surf*. 2013;11:236–245.
8. Millar TJ, Schuett BS. The real reason for having a meibomian lipid layer covering the outer surface of the tear film - A review. *Exp Eye Res*. 2015;137:125–138.
9. Svitova TF, Lin MC. Evaporation retardation by model tear-lipid films: the roles of film aging, compositions and interfacial rheological properties. *Colloids Surf. B*. 2021;197:111392.
10. Khanna RK, Catanese S, Emond P, Corcia P, Blasco H, Pisella PJ. Metabolomics and lipidomics approaches in human tears: a systematic review. *Surv Ophthalmol*. 2022;67:1229–1243.
11. Sheppard JD, Nichols KK. Dry eye disease associated with Meibomian gland dysfunction: focus on tear film characteristics and the therapeutic landscape. *Ophthalmol Ther*. 2023;12:1397–1418.
12. Suzuki T, Kitazawa K, Cho Y, et al. Alteration in meibum lipid composition and subjective symptoms due to aging and meibomian gland dysfunction. *Ocul Surf*. 2022;26:310–317.
13. Lam SM, Tong L, Yong SS, et al. Meibum lipid composition in Asians with dry eye disease. *PLoS One*. 2011;6:e24339.
14. Chen J, Green-Church KB, Nichols KK. Shotgun lipidomic analysis of human meibomian gland secretions with electrospray ionization tandem mass spectrometry. *Invest Ophthalmol Vis Sci*. 2010;51:6220–6231.
15. Sawai M, Watanabe K, Tanaka K, et al. Diverse meibum lipids produced by Awat1 and Awat2 are important for stabilizing tear film and protecting the ocular surface. *iScience*. 2021;24:102478.
16. Miyamoto M, Sassa T, Sawai M, Kihara A. Lipid polarity gradient formed by ω-hydroxy lipids in tear film prevents dry eye disease. *eLife*. 2020;9:e53582.
17. Butovich IA, Wilkerson A. Dynamic changes in the gene expression patterns and lipid profiles in the developing and maturing meibomian glands. *Int J Mol Sci*. 2022;23:7884.
18. Oelkers P, Behari A, Cromley D, Billheimer JT, Sturley SL. Characterization of two human genes encoding acyl coenzyme A: cholesterol acyltransferase-related enzymes. *J Biol Chem*. 1998;273:26765–26771.
19. Butovich IA, Wilkerson A, Yuksel S. Depletion of cholesteryl esters causes meibomian gland dysfunction-like symptoms in a Soat1-null mouse model. *Int J Mol Sci*. 2021;22:1583.
20. Widjaja-Adhi MAK, Chao K, Golczak M. Mouse models in studies on the etiology of evaporative dry eye disease. *Exp Eye Res*. 2022;219:109072.
21. Lu H, Wojtowicz JC, Butovich IA. Differential scanning calorimetric evaluation of human meibomian gland secretions and model lipid mixtures: transition temperatures and cooperativity of melting. *Chem Phys Lipids*. 2013;170-171:55–64.
22. Valle RP, Wu T, Zuo YY. Biophysical influence of airborne carbon nanomaterials on natural pulmonary surfactant. *Acs Nano*. 2015;9:5413–5421.
23. Rantamäki AH, Telenius J, Koivuniemi A, Vattulainen I, Holopainen JM. Lessons from the biophysics of interfaces: lung surfactant and tear fluid. *Prog Retin Eye Res*. 2011;30:204–215.
24. Xu X, Li G, Zuo YY. Biophysical properties of tear film lipid layer I. Surface tension and surface rheology. *Biophys J*. 2022;121:439–450.
25. Xu X, Kang C, Sun R, Zuo YY. Biophysical properties of tear film lipid layer II. Polymorphism of FAHFA. *Biophys J*. 2022;121:451–458.
26. Xu X, Li G, Zuo YY. Effect of model tear film lipid layer on water evaporation. *Invest Ophthalmol Vis Sci*. 2023;64:13.
27. Xu X, Zuo YY. Nanomedicine for ocular drug delivery. In: Gu N, ed. *Nanomedicine*. Singapore: Springer Nature Singapore; 2023:755–786.
28. Butovich IA, Wilkerson A, Bhat N, McMahon A, Yuksel S. On the pivotal role of Elovl3/ELOVL3 in meibogenesis and ocular physiology of mice. *FASEB J: Fed Am Soc Exp Biol*. 2019;33:10034–10048.
29. Yu K, Yang J, Zuo YY. Automated droplet manipulation using closed-loop axisymmetric drop shape analysis. *Langmuir*. 2016;32:4820–4826.
30. Yang J, Yu K, Tsuji T, Jha R, Zuo YY. Determining the surface dilational rheology of surfactant and protein films with a droplet waveform generator. *J Colloid Interface Sci*. 2019;537:547–553.
31. Mishima S, Gasset A, Klyce SD, Baum JL. Determination of tear volume and tear flow. *Invest Ophthalmol Vis Sci*. 1966;5:264–276.
32. Kim YH, Graham AD, Li W, Radke CJ, Lin MC. Human lacrimal production rate and wetted length of modified Schirmer's tear test strips. *Transl Vis Sci Technol*. 2019;8:40.
33. Oliveira ON, Caseli L, Ariga K. The past and the future of Langmuir and Langmuir-Blodgett films. *Chem Rev*. 2022;122:6459–6513.
34. Li G, Xu X, Zuo YY. Langmuir-Blodgett transfer from the oil-water interface. *J Colloid Interface Sci*. 2023;630:21–27.
35. Zuo YY, Veldhuizen RAW, Neumann AW, Petersen NO, Possmayer F. Current perspectives in pulmonary surfactant — Inhibition, enhancement and evaluation. *Biochim Biophys Acta (BBA) - Biomembr*. 2008;1778:1947–1977.
36. Tiffany JM. Surface tension in tears. *Arch Soc Esp Oftalmol*. 2006;81:363–366.
37. Marsh D. *Handbook of Lipid Bilayers*. 2nd ed. Boca Raton, FL: CRC Press; 2013.
38. Arciniega JC, Uchiyama E, Butovich IA. Disruption and destabilization of meibomian lipid films caused by increasing amounts of ceramides and cholesterol. *Invest Ophthalmol Vis Sci*. 2013;54:1352–1360.
39. Ipsen JH, Karlstrom G, Mouritsen OG, Wennerstrom H, Zuckermann MJ. Phase equilibria in the phosphatidylcholine-cholesterol system. *Biochimica et Biophysica Acta*. 1987;905:162–172.
40. Sankaram MB, Thompson TE. Cholesterol-induced fluid-phase immiscibility in membranes. *Proc Natl Acad Sci USA*. 1991;88:8686–8690.
41. Hung WC, Lee MT, Chen FY, Huang HW. The condensing effect of cholesterol in lipid bilayers. *Biophys J*. 2007;92:3960–3967.
42. de Meyer F, Smit B. Effect of cholesterol on the structure of a phospholipid bilayer. *Proc Natl Acad Sci*. 2009;106:3654–3658.
43. Zhang H, Wang YE, Neal CR, Zuo YY. Differential effects of cholesterol and budesonide on biophysical properties of clinical surfactant. *Pediatr Res*. 2012;71:316–323.
44. Leiske DL, Raju SR, Ketelson HA, Millar TJ, Fuller GG. The interfacial viscoelastic properties and structures of human and animal Meibomian lipids. *Exp Eye Res*. 2010;90:598–604.

Investigative Ophthalmology & Visual Science

45. Leiske D, Leiske C, Leiske D, et al. Temperature-induced transitions in the structure and interfacial rheology of human meibum. *Biophys J*. 2012;102:369–376.
46. Rosenfeld L, Cerretani C, Leiske DL, Toney MF, Radke CJ, Fuller GG. Structural and rheological properties of meibomian lipid. *Invest Ophthalmol Vis Sci*. 2013;54:2720–2732.
47. Miller R, Ferri JK, Javadi A, Krägel J, Mucic N, Wüstneck R. Rheology of interfacial layers. *Colloid Polym Sci*. 2010;288:937–950.
48. Georgiev GA, Yokoi N, Ivanova S, Tonchev V, Nencheva Y, Krastev R. Surface relaxations as a tool to distinguish the dynamic interfacial properties of films formed by normal and diseased meibomian lipids. *Soft Matter*. 2014;10:5579–5588.
49. Chhadva P, Goldhardt R, Galor A. Meibomian gland disease: the role of gland dysfunction in dry eye disease. *Ophthalmology*. 2017;124:S20–S26.
50. Baudouin C, Messmer EM, Aragona P, et al. Revisiting the vicious circle of dry eye disease: a focus on the pathophysiology of meibomian gland dysfunction. *Br J Ophthalmol*. 2016;100:300–306.
51. Pinna A, Blasetti F, Zinellu A, Carru C, Solinas G. Meibomian gland dysfunction and hypercholesterolemia. *Ophthalmology*. 2013;120:2385–2389.
52. Braich PS, Howard MK, Singh JS. Dyslipidemia and its association with meibomian gland dysfunction. *Int Ophthalmol*. 2016;36:469–476.
53. Tomioka Y, Kitazawa K, Yamashita Y, et al. Dyslipidemia exacerbates meibomian gland dysfunction: a systematic review and meta-analysis. *J Clin Med*. 2023;12:2131.
54. Nakayama N, Kawashima M, Kaido M, Arita R, Tsubota K. Analysis of meibum before and after intraductal meibomian gland probing in eyes with obstructive meibomian gland dysfunction. *Cornea*. 2015;34:1206–1208.
55. Mathers WD, Choi D. Cluster analysis of patients with ocular surface disease, blepharitis, and dry eye. *Arch Ophthalmol*. 2004;122:1700–1704.

Investigative Ophthalmology & Visual Science